arXiv:1404.3620v2 [math-ph] 16 Apr 2014

Viscous-Inviscid Interactions in a Boundary-Layer Flow Induced by a Vortex Array

F. Gargano[1,2], M. Sammartino[1], V. Sciacca[1], K.W Cassel[3]

[1]National Research Council (CNR), Institute for Coastal Marine Environment (IAMC), Via L. Vaccara 61, 91026, Mazara del Vallo (TP), Italy.

[2]Dept of Mathematics and Computer Science, University of Palermo Via Archirafi 34, 90123 Palermo, Italy.

[3]Department of Mechanical, Materials, and Aerospace Engineering, Illinois Institute of Technology, 10 West 32nd Street, Chicago, Illinois, USA.

Email addresses:
francesco.gargano@unipa.it (F.G),
marco@math.unipa.it (M.S.),
sciacca@math.unipa.it (V.S),
cassel@iit.edu (K.C)

Abstract

In this paper we investigate the asymptotic validity of boundary layer theory. For a flow induced by a periodic row of point-vortices, we compare Prandtl's solution to Navier-Stokes solutions at different Re numbers. We show how Prandtl's solution develops a finite time separation singularity. On the other hand Navier-Stokes solution is characterized by the presence of two kinds of viscous-inviscid interactions between the boundary layer and the outer flow. These interactions can be detected by the analysis of the enstrophy and of the pressure gradient on the wall. Moreover we apply the complex singularity tracking method to Prandtl and Navier-Stokes solutions and analyze the previous interactions from a different perspective.

1 Introduction

The study of the behavior of a high Reynolds number (Re) fluid interacting with a solid boundary is a central problem in the mathematical analysis of fluid dynamics. Due to the no-slip boundary condition, the convergence of Navier-Stokes (NS) solution to Euler solution, as $Re \to \infty$, fails, and Prandtl boundary layer equations must be used to resolve the flow close to the boundary. We mention the papers [36, 37, 3, 24] where, for analytic initial data, the authors prove the convergence of NS solutions to Euler and Prandtl. The zero viscosity limit was also considered in [18, 40, 20], where the authors introduce criteria based on a priori estimates of energy dissipation in a viscous sub layer, and in [29] where the author employs the assumption that, initially, the vorticity close to the boundary is zero. Strong convergence of Navier-Stokes to Euler solutions in L^2 spaces is given in [26, 27] with a symmetry assumption. In [8, 28, 19, 17, 43,

1, 2, 30, 10], the authors study the inviscid limit of the two-dimensional Navier-Stokes equations in the case of a Navier friction boundary condition. Conditions on the well-posedness of Prandtl's equation are given in [4, 25, 44, 22, 5], while results on the ill-posedness are in [15, 16]. The problem of the well posedness of Prandtl's equation is also related to the finite time singularity formation that has been observed for many significant flows (see for example [41, 34, 6]). At the singularity time the normal component of the velocity becomes infinite with ejection of vorticity and flow particles from within the boundary layer into the outer flow; the consequent breakdown of the assumptions on which Prandtl's equation are based on signals the limit of the classical boundary layer theory. However Prandtl and NS solutions begin to show a quantitative disagreement prior to Prandtl singularity formation: in fact, various interactions between the viscous boundary layer and the inviscid outer flow develop in NS flow. These interactions behave in a different manner from that observed in the Prandtl boundary-layer, and as observed in other initial flows (see [6, 13, 14]), they act over different length scales and they influence the flow evolution in a very different manner. The first interaction, called large-scale (LS) interaction, is found to occur for all finite Reynolds numbers, and it signals the time when the comparison between Navier-Stokes and Prandtl's solutions begins to show some quantitative discrepancies. The small-scale (SS) interaction develops only for moderate to high Reynolds numbers (generally $Re \geq O(10^4)$). This interaction is marked by large gradients along the streamwise to the boundary variable, a chaotic formation of small-scale vortical structures and a large amount of vorticity production on the boundary that, in turn, leads to the growth of enstrophy. This growth, caused by the collision on the wall of the various vortical structures that forms during the separation process, is absent both in Prandtl solutions as well in NS solutions for low Re.
In this paper we shall investigate these interactions in a flow induced by a vortex array.

2 Statement of the problem and numerical procedures

Our case study consists of an infinite row of point-vortices immersed in a 2D viscous incompressible flow at rest at infinity and bounded by an infinite rectilinear wall. In a cartesian frame the vortices are centered in $(ma + \pi,\, b)_{m\epsilon\mathbb{Z}}$, where b is the distance of the row from the wall and a is the distance of between two consecutive vortices. All the vortices have strength k. We study the system in the reference frame comoving with the vortices. The initial data for the streamwise and normal velocity components are $u_0 = \partial_y \Psi_E, v_0 = -\partial_x \Psi_E$, where

$$\Psi_E(x,y) = -U_c y - \frac{k}{4\pi}\log\left(\frac{\cosh(\frac{2\pi}{a}(y-b/2)) - \cos(\frac{2\pi}{a}(x-\pi))}{\cosh(\frac{2\pi}{a}(y+b/2)) - \cos(\frac{2\pi}{a}(x-\pi))}\right) \qquad (1)$$

is the streamfunction of the inviscid steady Euler solution for the vorticity configuration described above, while $U_c = \frac{k}{2a}\cosh(\pi b/a)$, see [23]. This is an a-periodic datum, and the velocity components obtained are such that $u = k/a$, $v = 0$ at $y = 0$, $u, v \to 0$ for $y \to \infty$. We set $a = 2\pi, k = 2a$ and we solve our

problem in the domain [0,2π]x[0,∞). Using b and U_c as characteristic length and velocity, NS equations in the vorticity-streamfunction formulation are:

$$\begin{aligned}
\frac{\partial \omega}{\partial t} + u\frac{\partial \omega}{\partial x} + v\frac{\partial \omega}{\partial y} &= \frac{1}{Re}\Delta\omega, && (2)\\
\Delta\psi &= -\omega, && (3)\\
u = \frac{\partial \psi}{\partial y}, \quad v &= -\frac{\partial \psi}{\partial x}, && (4)\\
\omega(x, y, t = 0) = \omega_0 &= 4\pi\delta_{(\pi,1)}, \quad \psi(x, y, 0) = \Psi_E && (5)\\
\omega(x, y \to \infty, 0) &= 0, \quad \omega(0, y, t) = \omega(2\pi, y, t) && (6)\\
u(x, 0, t) = -\coth(1), \quad v(x, 0, t) &= 0. && (7)
\end{aligned}$$

In the above equations the Reynolds number is defined as $Re = bU_c/\nu$, being ν the kinematic viscosity.

The initial vorticity is singular and to avoid this initial singularity we approximate the initial solution by convolving it with the gaussian mollifier $\Phi^\sigma(x, y) = \frac{1}{\sigma^2\pi}e^{-\frac{(x^2+y^2)}{\sigma^2}}$, obtaining the regularized vorticity $\omega^\sigma = \omega_0 * \Phi^\sigma = 4\pi\Phi^\sigma(x-\pi, y-1)$. This is a typical procedure used in computational vortex methods when the initial data have point singularities (as in [13]) or for vortex-sheet motion (as in [38]). In the NS calculations we have chosen $\sigma^2 = 5 \times 10^{-3}$. As $\psi \to \infty$ for $y \to \infty$ we truncate the computational domain at a finite value $y_{\max}$ of the normal variable. Following what proposed in [13] for the rectilinear vortex case, we chose this value requiring that the vorticity remains negligible for $y \geqslant y_{\max}$ for all computational time. We take $y_{\max} = 6$ for all the Re numbers, which we find to be large enough to satisfy the required condition for the vorticity as we have checked that for $y > 6$ no relevant differences arise between the various solutions.

Prandtl's equations for this setup are:

$$\begin{aligned}
\frac{\partial u}{\partial t} + u\frac{\partial u}{\partial x} + V\frac{\partial u}{\partial Y} - U_\infty\frac{\partial U_\infty}{\partial x} &= \frac{\partial^2 u}{\partial Y^2}, && (8)\\
\frac{\partial u}{\partial x} + \frac{\partial V}{\partial Y} &= 0, u(x, Y, 0) = U_\infty, && (9)\\
u(x, 0, t) &= -\coth(1), \quad u(x, Y \to \infty, t) = U_\infty, && (10)\\
u(0, y, t) &= u(2\pi, y, t), && (11)
\end{aligned}$$

where $U_\infty = \partial_y \Psi_{E|y=0}$ is the inviscid solution of the outer flow.

The system (2)-(7) is solved with a Galerkin-Fourier method in the streamwise variable, while the Chebyshev-collocation method is used in the normal variable. This ensures fully spectral convergence, see [35]. The temporal discretization used is the Adams-Bashforth-Implicit Backward Differentiation method, and to find the necessary vorticity boundary condition, the influence matrix method [35] is used. The description of the numerical techniques used to treat the initial singular vorticity and the infinite normal domain can be found in [13]. Numerical solutions for Reynolds numbers ranging from 10^3 up to $5 \cdot 10^4$ are computed, with computational grids up to 8192×1025 points for the higher Reynolds numbers. To solve Prandtl system (8)-(11) we have used the fully spectral numerical scheme used in [12] and a computational grids up to 4096×1025 points.

3 Prandtl's Solution

In this section we shall describe the main physical events leading to singularity formation for Prandtl's equation, and we shall apply the singularity tracking method to detect the time at which singularity forms.

The formation of a recirculation eddy detached from the wall is the first relevant physical event in Prandtl's solution. It occurs at $t \approx 0.28$, and it is due to the adverse streamwise pressure gradient (the term $U_\infty \frac{\partial U_\infty}{\partial x}$ in (8)) imposed by the outer flow . This recirculation region can be observed in Fig.1(a) where the Prandtl's vorticity $\omega_P = -\partial_Y u$ is shown at $t = 0.5$, along with some pathlines of fluid particles followed from $t = 0.4$ up to $t = 0.5$. The pathlines rotate clockwise above the zone of positive vorticity where the recirculation region is formed. As time passes this eddy thickens rapidly in the streamwise direction, and a spike in vorticity contours forms at $t \approx 0.86$. This is visible in Fig.1(b) at $t = 1$ where also the pathlines are shown: the pathlines experience a rapid transition in the normal direction, meaning that fluid particles are ejected from within the boundary layer to the outer flow.

To characterize the singularity of Prandtl's solution, we apply the singularity tracking method (see [39]). This method has been widely used to characterize the singularity formation for ODEs and PDEs (see [39, 42, 33, 11, 12, 9]). We write the Fourier-Chebyshev expansion of Prandtl's solution (see [12] for the details):

$$u(x, y, t) \approx \sum_{k=-M/2}^{k=M/2} \sum_{j=0}^{j=N} u_{kj}(t) e^{ik\theta} T_j(y) \, , \tag{12}$$

where $T_j(y)$ are Chebyshev polynomials of the first kind. In this way we can apply the singularity tracking method to the shell-summed Fourier amplitudes defined as

$$A_K \equiv \sum_{K \le |(k,j)| < K+1} |u_{k,j}|, \tag{13}$$

which have the following asymptotic behavior ([33]):

$$A_K \approx C K^{-(\alpha_P+1)} \exp(-\delta_P K), \quad \text{for } K \to \infty. \tag{14}$$

In the above formula δ_P gives the width of the analyticity strip while the algebraic prefactor α_P gives informations on the nature of the singularity. By performing a fitting procedure on the parameters δ_P and α_P, we find that $\delta_P \approx 0$ at $t_s \approx 1$, revealing the singularity formation, while the characterization of the singularity at t_s is $\alpha_P \approx 1/3$. We notice that the characterization $\alpha_P \approx 1/3$ is the same obtained in [12] for the impulsively started disk.

4 Navier–Stokes Solution

In this section we compare Navier-Stokes solutions at different Re numbers ($10^3, 10^4$ and $5 \cdot 10^4$), with the solution of the boundary layer equations. Moreover we shall describe the viscous–inviscid interactions between the viscous boundary layer and the outer flow which characterize Navier-Stokes solutions.

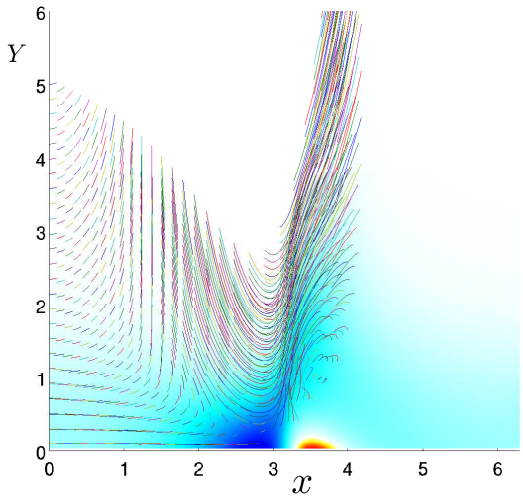

(a) $t = 0.5$

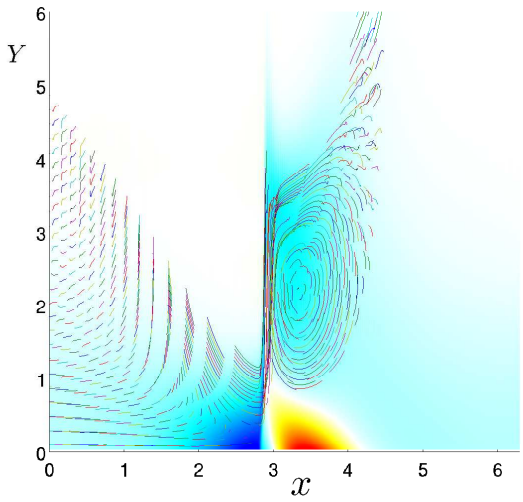

(b) $t = 1$

Figure 1: The vorticity contour levels of Prandtl's solution at time $t = 0.5$ and time $t = 1$ (red colors positive vorticity, blue color negative vorticity). In these figures the pathlines of flow particles are also show. In a) the recirculation region has already formed, and the pathlines followed from $t = 0.4$ to $t = 0.5$, begin to rotate clockwise in the region above the positive vorticity. In b), just prior the singularity formation, a spike is visible in the vorticity contour, and the pathlines, followed from $t = 0.9$ to $t = 1$ experience a rapid transition in the normal direction in the streamwise position $x_s \approx 2.86$

4.1 LS interaction

In the literature of the recent years it was proposed to analyze the streamwise pressure gradient $\partial_x p_w = -\frac{1}{Re}\partial_y \omega|_{y=0}$ at the wall in order to evaluate when the viscous–inviscid interaction begins: this was performed in [6, 31] for the thick core vortex case, and in [13] for the rectilinear vortex. The idea behind this approach lies in the fact that for Prandtl's equation the streamwise pressure gradient is imposed by the outer flow and, in the case of stationary Euler solution, it is constant in time: therefore any variations of $\partial_x p_w$ in Navier-Stokes solution is a good indicator of the beginning of the viscous-inviscid interaction. In Figs.2(a)-2(b) we show the time evolution of $\partial_x p_w$ starting at $t = 0.2$ until $t = 0.5$, with increments of 0.1 for $Re = 10^3, 5 \cdot 10^4$. It was proposed in [13] that the interaction begins when an inflection point in $\partial_x p_w$ forms close to its maximum, and in this case this happens at time $t_{LS} \approx 0.33, 0.34, 0.38$ for $Re = 10^3, 10^4, 5 \cdot 10^4$ respectively. The time of this first interaction, which in the literature is known as large–scale (LS) interaction scale , is quite early with respect to theoretical prediction of boundary layer theory, according to which the viscous–inviscid interaction begins at the singularity time. Moreover LS-interaction has no resemblance with the viscous-inviscid interaction developed by Prandtl's solution at t_s: in fact no vorticity ejection from the boundary layer is visible, and no large gradient in the streamwise variable forms. For instance in Fig.3(a) the vorticity is shown at $t = 0.5$ along with the pathlines of same particles fluid followed from $t = 0.4$ to $t = 0.5$: no vorticity ejection phenomena are visible (they appear at later time) and no spiky behavior is visible in the vorticity as it happens in Prandtl's vorticity at t_s (see Fig.1(b)).

4.2 SS interaction

The LS-interaction is the precursor, in the case of moderate–high Re numbers ($Re \geq O(10^4)$), of another interaction acting on a smaller scale (SS-interaction). This new interaction is characterized by the formation of large gradients in the streamwise variable and, physically, by the continuous formation of small-scale vortical structures within the boundary layer. These structures first separate from the wall; then, due to their reciprocal interactions, they are driven back toward the wall, leading to a large vorticity production and the consequent growth of the enstrophy and decrease of energy. To show how the evolution of the enstrophy is a good indicator of this phenomenology, we write the equation governing the enstrophy evolution in the boundary layer $D = [0, 2\pi] \times [0, Y_{BL}]$ where Y_{BL} is large enough so that all the relevant phenomena occurring in the boundary layer are captured. This equation is:

$$\frac{d\Omega(t)}{dt} = -\frac{2}{Re}\|\nabla\omega\|^2_{L^2(D)} + 2I^p(t) + NT \tag{15}$$

where $\Omega(t) = \|\omega\|^2_{L^2(D)}$ and:

$$I^p(t) = \int_0^{2\pi} \omega_{|y=0} \cdot \partial_x p_w dx, \quad NT = \frac{2}{Re}\int_0^{2\pi} (\omega \cdot \partial_y \omega)_{|y=Y_{BL}}\, dx\ .$$

The NT term is negligible because at $y = Y_{BL}$ the vorticity ω is very small, and therefore we shall not consider this terms in the rest of our analysis. The only

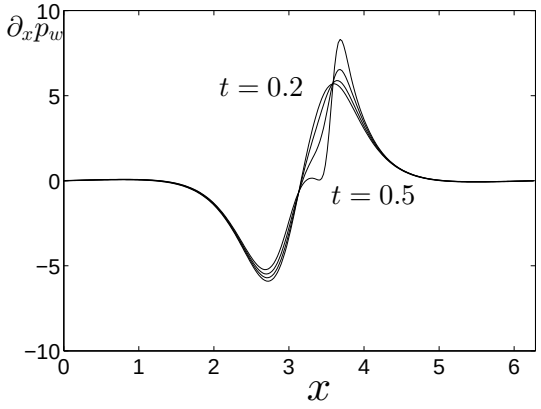

(a) $Re = 10^3$

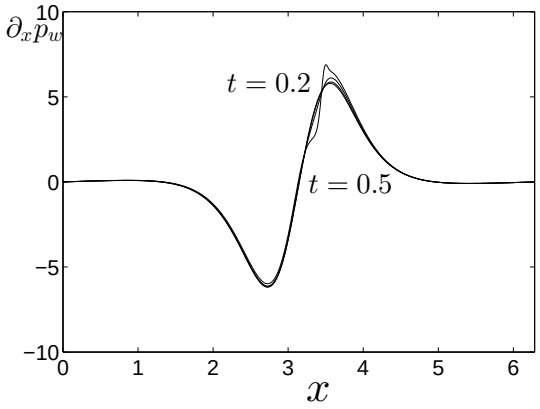

(b) $Re = 5 \cdot 10^4$

Figure 2: The time evolution of $\partial_x p_w$ for $Re = 10^3, 5 \cdot 10^4$ number (time step of 0.1). Large–scale interaction begins when an inflection point forms in $\partial_x p_w$, and this happens at time $t_{LS} \approx 0.33, 0.38$ for $Re = 10^3, 5 \cdot 10^4$ respectively.

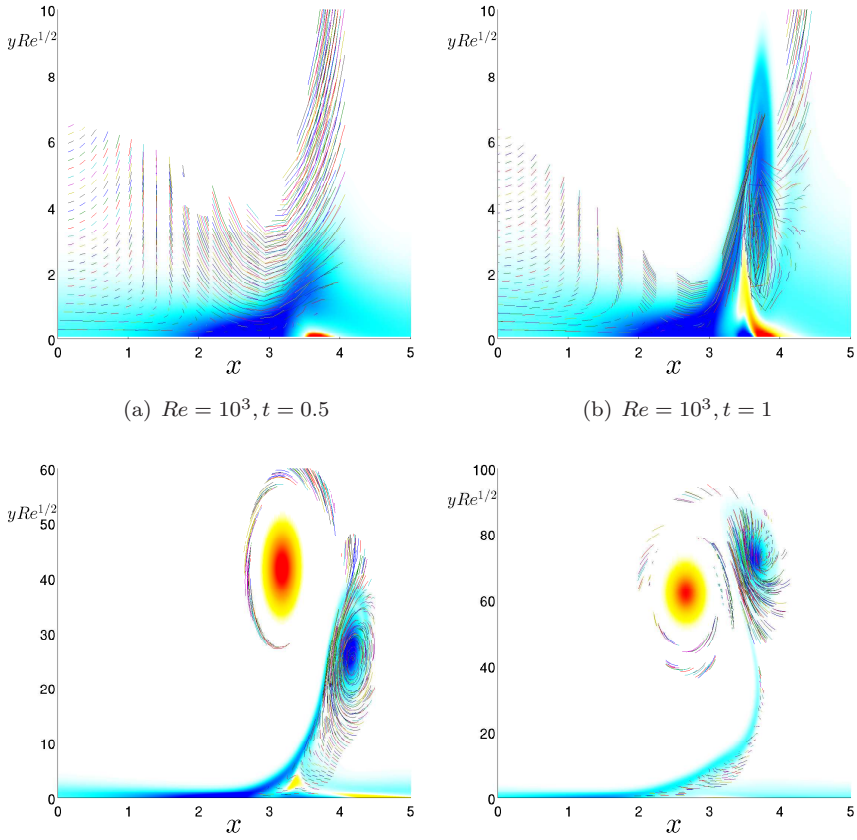

(a) $Re = 10^3, t = 0.5$ (b) $Re = 10^3, t = 1$

(c) $Re = 10^3, t = 2$ (d) $Re = 10^3, t = 3$

Figure 3: The vorticity (red colors positive vorticity, blue color negative vorticity) and the pathlines of fluid particles for $Re = 10^3$ at time $t = 0.5, 1, 2, 3$. The pathlines are followed in temporal intervals $[0.4, 0.5], [0.9, 1], [1.9, 2], [2.9, 3]$. A big core of negative vorticity detaches from the wall and moves toward the main vortex. During its motion this big core never impinges on the wall, and no other vortical structures detach from the wall.

way for the enstrophy to increase is via the integral term I^p which is related to the vorticity and to the vorticity flux at the boundary: when a vortical structure impinges on the wall a large amount of vorticity is produced and the enstrophy therefore grows. In Fig.15 it is shown the enstrophy evolution for Prandtl's solution and for the various NS solutions (in this case we rescale the enstrophy with a factor $Re^{-1/2}$). While for Prandtl and NS at $Re = 10^3$ the enstrophy decreases monotonically, several peaks are present for $Re = 10^4, 5 \cdot 10^4$. For these high Re numbers the vortical structures form continuously and after the detachment from the boundary they impinge on the wall. This leads to a strong ejection of flow particles from the boundary and the growth of the enstrophy (see Figs.4(a)-(d) for the pathlines and the vorticity contour at $Re = 10^4$). On the other hand, the behavior at lower Re numbers is quite different. In fact for $Re = 10^3$ the enstrophy decreases because the big core of negative vorticity that form during the separation process, visible in Figs.3(a)-3(d) at different times, detaches from the wall, moves toward the main vortex until they interact, and does not impinge on the wall. This different temporal behavior of the enstrophy for the two Re number regimes was also observed for the rectilinear vortex case [13], and for a dipole-vortex [21, 32]. We observe that the first peak in the enstrophy evolution forms earlier for $Re = 5 \cdot 10^4$ than for $Re = 10^4$, although the LS-interaction forms earlier for $Re = 10^4$. This confirms what observed in [6, 13] for other flow, i.e. that the LS-interaction formation strongly accelerates the SS-interaction because the temporal gap between the beginning of the two interaction decreases as Re increases.
The physical effects of the SS-interaction have similarities with the effect due to the singularity formation for Prandtl's equation: in fact, there are large gradients forming in the solution in the streamwise variable, and a strong eruption of flow particles from the boundary layer. This leads to the conjecture that as $Re \to \infty$, LS and SS interactions merge together and they are a unique interaction forming at the time at which Prandtl's singularity occurs. To give strength to this conjecture we can perform the singularity analysis to NS solution, and in particular we analyze the streamwise velocity component u of NS solution within the boundary region D defined at the beginning of this section. We track the the width of analyticity strip δ_{NS} and the characterization α_{NS} of the main complex singularity of the solution by applying the singularity tracking method. In Fig.4.2 we can observe that $\delta_{NS}(t)$ has a minimum δ^m_{NS} that forms closer to t_s as Re increases. We can therefore expect that as $Re \to \infty$ the main complex singularity of NS solution behaves like Prandtl's singularity and $\delta^m_{NS} \to 0$ as $Re \to \infty$. Regarding the characterization α_{NS} we find for all the Re that $\alpha_{NS} \approx 1/2$, while $\alpha_P \approx 1/3$. A similar characterization was also detected in [14] for impulsively started disk initial datum. In this work it was supposed that α_{NS} and α_P are strongly influenced by the viscous-inviscid interactions occurring during the flow evolution. Therefore a discrepancy between the values α_{NS} and α_P is likely to occur.

5 Conclusion

We have computed the solutions of 2D Prandtl and Navier-Stokes equations in the the case of a vortex array interacting with a wall. Prandtl's equations develop a separation singularity at $t_s \approx 1$. The unsteady separation process for

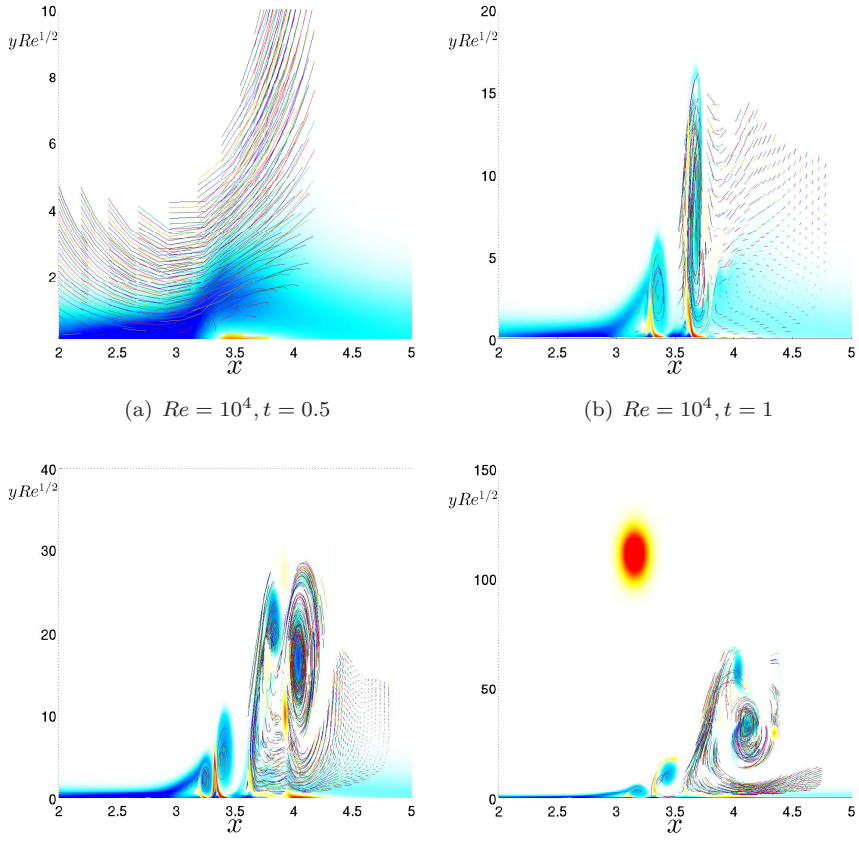

(a) $Re = 10^4, t = 0.5$

(b) $Re = 10^4, t = 1$

(c) $Re = 10^4, t = 2$

(d) $Re = 10^4, t = 3$

Figure 4: The vorticity (red colors positive vorticity, blue color negative vorticity) and the pathlines of fluid particles for $Re = 10^4$ at time $t = 0.5, 1, 1.5, 2$. The pathlines are followed in the temporal intervals $[0.4, 0.5]$, $[0.9, 1]$, $[1.4, 1.5]$, $[1.9, 2]$. Several cores of negative vorticity detach from the wall and moves toward the main vortex. During their motion these structures impinge on the wall leading to the growth of the enstrophy (see Fig.5).

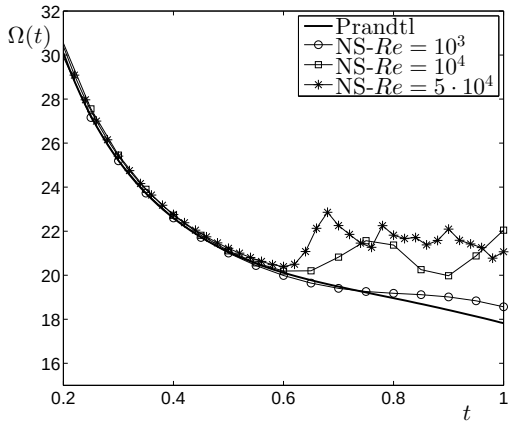

Figure 5: The temporal evolution of Prandtl enstrophy $\Omega_P(t) = \|\partial_Y u\|^2_{L^2}$ and the rescaled NS enstrophy $\Omega(t)/\sqrt{Re}$ at different Re number. Up to LS-interaction the good comparison reflects the good agreement between NS and Prandtl's solutions. During the SS-interaction the enstrophy for $Re = 10^4 - 5 \cdot 10^4$ strongly differ from the cases $Re = 10^3$ and Prandtl: this is due to the interactions of the vortical structures within the boundary layer.

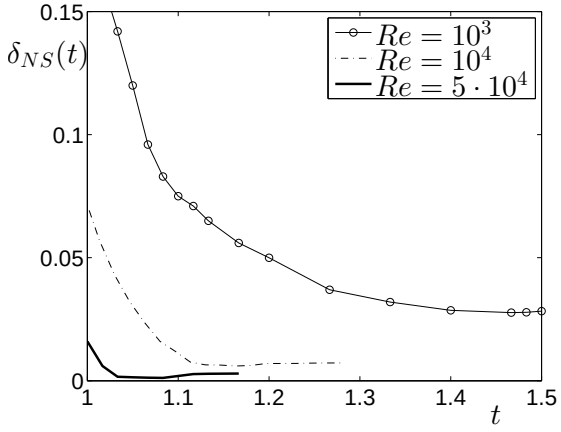

Figure 6: Temporal evolution of δ_{NS} for various Reynolds number. At time $t_s = 1$, δ_{NS} approaches zero as Reynolds number increases. Then it reaches a minimum (δ^m_{NS}) . The time at which δ^m_{NS} forms becomes closer to t_s as Reynolds number increases.

Navier-Stokes solutions reveals a different behavior from Prandtl's case. In particular there are two kinds of interaction between the viscous boundary layer and the inviscid outer flow . The LS interactions is found to occur for all Reynolds numbers considered, and it is characterized by discrepancies arising between the streamwise pressure gradient at the wall and the same quantity imposed by Prandtl's solution. The SS interaction occurs only for moderate to high Reynolds numbers ($Re \geq O(10^4)$), and it is marked by the formation of large gradients in the streamwise variable, and the formation of vortical structures within the boundary layer leading to a complicate flow dynamics revealed also by the growth of the enstrophy. This growth, caused by the collision of the vortical structures on the wall, is absent both in Prandtl solutions as well in NS solutions for low Re number.
The various interactions occurring in Prandtl and Navier-Stokes solutions have been investigated by performing a complex singularity analysis on the streamwise velocity component u. This analysis shows that Prandtl's singularity can be characterized as a cubic-root singularity. On the other hand the width of the analyticity strip of the Navier-Stokes solutions reaches a minimum value δ^m_{NS} decreasing as Reynolds increases, and it forms in a time which is closer to t_s as Reynolds number increases, supporting the conjecture that $\delta^m_{NS} \to 0$ at t_s as $Re \to \infty$. The primary difference between the analysis of the spectrum of u as compared to that from Prandtl's solution is the characterization obtained from the rate of algebraic decay of the shell summed amplitudes. For Navier-Stokes solutions it has been found that $\alpha^{NS} \approx 1/2$ for all Reynolds numbers considered, while the prediction of boundary-layer theory is that $\alpha^P \approx 1/3$. This discrepancy can be explained by the presence of the LS and SS interactions that act in a different manner on the flow evolution as compared to the viscous-inviscid interaction present as $Re \to \infty$. We plan to investigate on the characterization of Navier-Stokes main complex singularity for very high Re numbers ($Re \geq 10^6$). Moreover these very high Re are characterized by the possible presence of a Rayleigh instability (observed in [7] for the thick-core vortex case): it is our intention to detect if this instability is present also for other initial data and if there is any link with the complex singularity of Navier-Stokes solution.

References

[1] H. Beirão da Veiga and F. Crispo. Concerning the $W^{k,p}$-inviscid limit for 3-D flows under a slip boundary condition. *J. Math. Fluid. Mech.*, 13:117–135, 2011.

[2] H. Beirão da Veiga and F. Crispo. The 3D inviscid limit result under slip boundary conditions. a negative answer. *J. Math. Fluid. Mech.*, 14:55–59, 2012.

[3] R. Caflisch and M. Sammartino. Navier-Stokes equations on an exterior circular domain: construction of the solution and the zero viscosity limit. *Comptes Rendus de l'Académie des Sciences - Series I - Mathematics*, 324(8):861 – 866, 1997.

[4] M. Cannone, M.C. Lombardo, and M. Sammartino. Existence and uniqueness for the Prandtl equations. *Comptes Rendus de l'Académie des Sciences - Series I - Mathematics*, 332(3):277 – 282, 2001.

[5] M. Cannone, M.C. Lombardo, and M. Sammartino. Well-posedness of Prandtl equations with non-compatible data. *Nonlinearity*, 26(3):3077–3100, 2013.

[6] K.W. Cassel. A comparison of Navier-Stokes solutions with the theoretical description of unsteady separation. *Phil. Trans. R. Soc. Lond. A.*, 358:3207–3227, 2000.

[7] K.W. Cassel and A.V. Obabko. A Rayleigh instability in a vortex-induced unsteady boundary layer. *Physica Scripta*, 2010(T142):014006, 2010.

[8] T. Clopeau, A. Mikelic, and R. Robert. On the vanishing viscosity limit for the 2d incompressible navier-stokes equations with the friction type boundary conditions. *Nonlinearity*, 11(6):1625–1636, 1998.

[9] G.M. Coclite, F. Gargano, and V. Sciacca. Analytic solutions and singularity formation for the peakon b-family equations. *Acta Appl. Math.*, 122:419–434, 2012.

[10] P. Constantin, I. Kukavica, and V. Vicol. On the inviscid limit of the Navier-Stokes equations. *arXiv:1403.5748v1*, 2014.

[11] G. Della Rocca, M.C. Lombardo, M. Sammartino, and V. Sciacca. Singularity tracking for Camassa-Holm and Prandtl's equations. *Appl. Numer. Math.*, 56(8):1108–1122, 2006.

[12] F. Gargano, M. Sammartino, and V. Sciacca. Singularity formation for Prandtl's equations. *Physica D: Nonlinear Phenomena*, 238(19):1975–1991, 2009.

[13] F. Gargano, M. Sammartino, and V. Sciacca. High Reynolds number Navier-Stokes solutions and boundary layer separation induced by a rectilinear vortex. *Computers & Fluids*, 52:73–91, 2011.

[14] F. Gargano, M. Sammartino, V. Sciacca, and K.W. Cassel. Analysis of complex singularities in high-Reynolds-number Navier-Stokes solutions. *In press on J. Fluid. Mech., doi:10.1017/jfm.2014.153, arXiv:1310.3943.*

[15] D. Gerard-Varet and E. Dormy. On the ill-posedness of the Prandtl equation. *J. Am. Math. Soc.*, 23:591–609, 2010.

[16] D. Gerard-Varet and T. Nguyen. Remarks on the ill-posedness of the Prandtl equation. *Asymptot. anal.*, 77:71–88, 2012.

[17] D. Iftimie and G. Planas. Inviscid limits for the Navier-Stokes equations with Navier friction boundary conditions. *Nonlinearity*, 19:899–918, 2006.

[18] T. Kato. *Remarks on the Zero Viscosity Limit for Nonstationary Navier-Stokes Flows with Boundary*, volume 2. Springer, New York, 1984.

[19] J.P. Kelliher. Navier-Stokes equations with Navier boundary conditions for bounded domain in the plane. *J. Math. Anals.*, 38:210–232, 2006.

[20] J.P. Kelliher. On Kato's conditions for vanishing viscosity. *Indiana Univ. Math. J.*, 56(4):1711–1721, 2007.

[21] W. Kramer, H.J.H. Clercx, , and G.J.F. van Heijst. Vorticity dynamics of a dipole colliding with a no-slip wall. *Physics of Fluids*, 19(12):126603, 2007.

[22] I. Kukavica and V. Vicol. On the local existence of analytic solutions to the Prandtl boundary layer equations. *Commun. Math. Sci.*, 11:269–292, 2013.

[23] H. Lamb. *Hydrodynamics*. Cambridge Mathematical Library. Cambridge University Press, Cambridge, sixth edition, 1993. With a foreword by R. A. Caflisch [Russel E. Caflisch].

[24] M.C. Lombardo, R.E. Caflisch, and M. Sammartino. Asymptotic analysis of the linearized Navier-Stokes equation on an exterior circular domain: Explicit solution and the zero viscosity limit. *Communications in Partial Differential Equations*, 26(1-2):335–354, 2001.

[25] M.C. Lombardo, M. Cannone, and M. Sammartino. Well-posedness of the boundary layer equations. *SIAM J. Math. Anal.*, 35(4):987–1004 (electronic), 2003.

[26] M.C. Lopes Filho, A.L. Mazzucato, and H.J. Nussenzveig Lopes. Vanishing viscosity limit for incompressible flow inside a rotating circle. *Physica D: Nonlinear Phenomena*, 237(10-12):1324–1333, 2008.

[27] M.C. Lopes Filho, A.L. Mazzucato, H.J. Nussenzveig Lopes, and M. Taylor. Vanishing viscosity limits and boundary layers for circularly symmetric 2D flows. *Bull. Braz. Math. Soc.*, 39:471–513, 2008.

[28] M.C Lopes Filho, H. Nussenzveig Lopes, and G. Planas. On the inviscid limit for two-dimensional incompressible flow with navier friction condition. *SIAM Journal on Mathematical Analysis*, 36(4):1130–1141, 2005.

[29] Y. Maekawa. Solution formula for the vorticity equations in the half plane with application to high vorticity creation at zero viscosity limit. *Adv. Diff. Eqns*, 18:101–146, 2013.

[30] N.Masmoudi and F.Rousset. Uniform regularity for the Navier-Stokes equation with Navier boundary condition. *Arch. Ration. Mech. Anal.*, 203:529–75, 2012.

[31] A.V. Obabko and K.W. Cassel. Navier-Stokes solutions of unsteady separation induced by a vortex. *J. Fluid Mech.*, 465:99–130, 2002.

[32] P. Orlandi. Vortex dipole rebound from a wall. *Physics of Fluids A: Fluid Dynamics*, 2(8):1429–1436, 1990.

[33] W. Pauls, T. Matsumoto, U. Frisch, and J. Bec. Nature of Complex Singularities for the 2D Euler Equation. *Physica D*, 219(1):40–59, 2006.

[34] V.J. Peridier, F.T. Smith, and J.D.A Walker. Vortex-induced boundary-layer separation. Part 1. The unsteady limit problem $Re \to \infty$. *J. Fluid Mech.*, 232:99–131, 1991.

[35] R. Peyret. *Spectral Methods for Incompressible Viscous Flow.* Springer-Verlag, New York, 2002.

[36] M. Sammartino and R.E. Caflisch. Zero viscosity limit for analytic solutions, of the Navier-Stokes equation on a half-space. I. Existence for Euler and Prandtl equations. *Comm. Math. Phys.*, 192(2):433–461, 1998.

[37] M. Sammartino and R.E. Caflisch. Zero viscosity limit for analytic solutions of the Navier-Stokes equation on a half-space. II. Construction of the Navier-Stokes solution. *Comm. Math. Phys.*, 192(2):463–491, 1998.

[38] M.J. Shelley. A study of singularity formation in vortex–sheet motion by a spectrally accurate vortex method. *J. Fluid. Mech.*, 244:493–526, 1992.

[39] C. Sulem, P.L. Sulem, , and H. Frisch. Tracing complex singularities with spectral methods. *J. Comput. Phys.*, 50:138–161, 1983.

[40] R. Temam and X. Wang. The convergence of the solutions of the Navier-Stokes equations to that of the Euler equations. *App. Math. Lett.*, 10:29–33, 1997.

[41] L.L. van Dommelen and S.F. Shen. The spontaneous generation of the singularity in a separating laminar boundary layer. *J. Comp. Phys.*, 38:125–140, 1980.

[42] J.A.C. Weideman. Computing the Dynamics of Complex Singularities of Nonlinear PDEs. *J. Appl. Dynamical System*, 2(2):171–186, 2003.

[43] L. Whang, Z. Xin, and A. Zang. Vanishing viscous limits for 3D Navier-Stokes equations with a Navier-slip boundary condition. *J. Math. Fluid. Mech.*, 14:791–825, 2012.

[44] Z. Xin and L. Zhang. On the global existence of solutions to the Prandtl's system. *Adv. Math.*, 181(1):88–133, 2004.